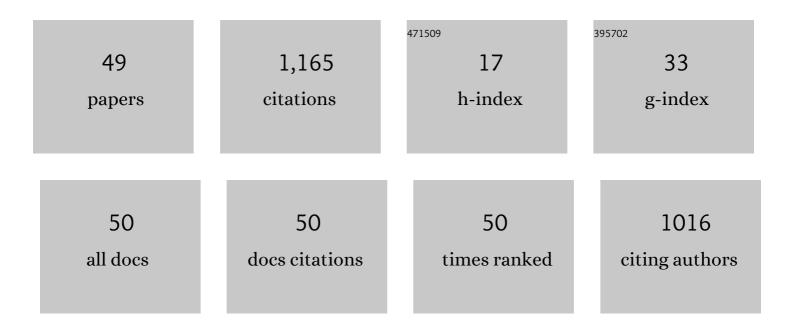
## Xiangyang Tang

List of Publications by Year in descending order

Source: https://exaly.com/author-pdf/7483117/publications.pdf Version: 2024-02-01



#	Article	IF	CITATIONS
1	Paired cycleâ€GANâ€based image correction for quantitative coneâ€beam computed tomography. Medical Physics, 2019, 46, 3998-4009.	3.0	164
2	Flat panel detector-based cone-beam volume CT angiography imaging: system evaluation. IEEE Transactions on Medical Imaging, 2000, 19, 949-963.	8.9	123
3	CBCTâ€based synthetic CT generation using deepâ€attention cycleGAN for pancreatic adaptive radiotherapy. Medical Physics, 2020, 47, 2472-2483.	3.0	113
4	A three-dimensional-weighted cone beam filtered backprojection (CB-FBP) algorithm for image reconstruction in volumetric CT—helical scanning. Physics in Medicine and Biology, 2006, 51, 855-874.	3.0	107
5	A three-dimensional weighted cone beam filtered backprojection (CB-FBP) algorithm for image reconstruction in volumetric CT under a circular source trajectory. Physics in Medicine and Biology, 2005, 50, 3889-3905.	3.0	74
6	Cone beam volume CT image artifacts caused by defective cells in x-ray flat panel imagers and the artifact removal using a wavelet-analysis-based algorithm. Medical Physics, 2001, 28, 812-825.	3.0	48
7	Characterization of imaging performance in differential phase contrast CT compared with the conventional CT—Noise power spectrum NPS( <i>k</i> ). Medical Physics, 2011, 38, 4386-4395.	3.0	43
8	3D Fusion of LV Venous Anatomy on Fluoroscopy Venograms With Epicardial Surface on SPECT Myocardial Perfusion Images for Guiding CRT LV Lead Placement. JACC: Cardiovascular Imaging, 2014, 7, 1239-1248.	5.3	43
9	Learningâ€based <scp>CBCT</scp> correction using alternating random forest based on autoâ€context model. Medical Physics, 2019, 46, 601-618.	3.0	36
10	CTâ€based multiâ€organ segmentation using a 3D selfâ€attention Uâ€net network for pancreatic radiotherapy. Medical Physics, 2020, 47, 4316-4324.	3.0	35
11	Characterization of imaging performance in differential phase contrast CT compared with the conventional CT: Spectrum of noise equivalent quanta NEQ( <i>k</i> ). Medical Physics, 2012, 39, 4467-4482.	3.0	33
12	A cone beam filtered backprojection (CBâ€FBP) reconstruction algorithm for a circleâ€plusâ€twoâ€arc orbit. Medical Physics, 2001, 28, 1042-1055.	3.0	31
13	Statistical CT noise reduction with multiscale decomposition and penalized weighted least squares in the projection domain. Medical Physics, 2012, 39, 5498-5512.	3.0	30
14	A filtered backprojection algorithm for cone beam reconstructionusing rotational filtering under helical source trajectory. Medical Physics, 2004, 31, 2949-2960.	3.0	26
15	On the data acquisition, image reconstruction, cone beam artifacts, and their suppression in axial <scp>MDCT</scp> and <scp>CBCT</scp> – A review. Medical Physics, 2018, 45, e761.	3.0	21
16	Optimal virtual monoenergetic image in "TwinBeam―dualâ€energy <scp>CT</scp> for organsâ€atâ€risk delineation based on contrastâ€noiseâ€ratio in headâ€andâ€neck radiotherapy. Journal of Applied Clinical Medical Physics, 2019, 20, 121-128.	1.9	21
17	Dosimetric study on learning-based cone-beam CT correction in adaptive radiation therapy. Medical Dosimetry, 2019, 44, e71-e79.	0.9	20
18	Increased Computed Tomography Dose Due to Miscentering With Use of Automated Tube Voltage Selection: Phantom and Patient Study. Current Problems in Diagnostic Radiology, 2016, 45, 265-270.	1.4	17

XIANGYANG TANG

#	Article	IF	CITATIONS
19	Prevalence and Severity of Off-Centering During Diagnostic CT: Observations From 57,621 CT scans of the Chest, Abdomen, and/or Pelvis. Current Problems in Diagnostic Radiology, 2019, 48, 229-234.	1.4	17
20	Enhancement of in-plane spatial resolution in volumetric computed tomography with focal spot wobbling – Overcoming the constraint on number of projection views per gantry rotation. Journal of X-Ray Science and Technology, 2010, 18, 251-265.	1.0	16
21	Optimization based beam-hardening correction in CT under data integral invariant constraint. Physics in Medicine and Biology, 2018, 63, 135015.	3.0	11
22	On the Conditioning of Spectral Channelization (Energy Binning) and Its Impact on Multi-Material Decomposition Based Spectral Imaging in Photon-Counting CT. IEEE Transactions on Biomedical Engineering, 2021, 68, 2678-2688.	4.2	11
23	A nanocomposite of Auâ€AgI core/shell dimer as a dualâ€modality contrast agent for xâ€ray computed tomography and photoacoustic imaging. Medical Physics, 2016, 43, 589-599.	3.0	10
24	Axial Cone-Beam Reconstruction by Weighted BPF/DBPF and Orthogonal Butterfly Filtering. IEEE Transactions on Biomedical Engineering, 2016, 63, 1895-1903.	4.2	10
25	Interior tomography in microscopic CT with image reconstruction constrained by full field of view scan at low spatial resolution. Physics in Medicine and Biology, 2018, 63, 075006.	3.0	10
26	On the conditioning of basis materials and its impact on multimaterial decompositionâ€based spectral imaging in photonâ€counting CT. Medical Physics, 2021, 48, 1100-1116.	3.0	10
27	The mathematical equivalence of consistency conditions in the divergent-beam computed tomography. Journal of X-Ray Science and Technology, 2012, 20, 45-68.	1.0	9
28	Principal Component Analysis in Projection and Image Domains—Another Form of Spectral Imaging in Photon-Counting CT. IEEE Transactions on Biomedical Engineering, 2021, 68, 1074-1083.	4.2	9
29	Improving image quality of cone-beam CT using alternating regression forest. , 2018, 10573, .		9
30	High through-plane resolution CT imaging with self-supervised deep learning. Physics in Medicine and Biology, 2021, 66, 145013.	3.0	8
31	Gratingâ€based xâ€ray differential phase contrast imaging with twin peaks in phaseâ€stepping curves—phase retrieval and dewrapping. Medical Physics, 2016, 43, 2855-2869.	3.0	6
32	Contentâ€oriented sparse representation ( <scp>COSR</scp> ) for <scp>CT</scp> denoising with preservation of texture and edge. Medical Physics, 2018, 45, 4942-4954.	3.0	6
33	Optimization of basis material selection and energy binning in three material decomposition for spectral imaging without contrast agents in photon-counting CT. , 2020, , .		6
34	Three-Dimensional Weighting in Cone Beam FBP Reconstruction and Its Transformation Over Geometries. IEEE Transactions on Biomedical Engineering, 2018, 65, 1235-1244.	4.2	5
35	X-ray differential phase contrast and dark-field computed tomography and radiography with microbubbles as contrast agent. , 2013, , .		4
36	Complex dark-field contrast and its retrieval in x-ray phase contrast imaging implemented with Talbot interferometry. Medical Physics, 2014, 41, 101914.	3.0	4

XIANGYANG TANG

#	Article	IF	CITATIONS
37	Reducing radiation dose in grating based xâ€ray phase contrast CT with twinâ€peaks in its phase stepping curves. Medical Physics, 2016, 43, 5942-5950.	3.0	4
38	A patch-based CBCT scatter artifact correction using prior CT. Proceedings of SPIE, 2017, 10132, .	0.8	4
39	Optimization of data acquisition in axial <scp>CT</scp> under the framework of sampling on lattice for suppression of aliasing artifacts with algorithmic detector interlacing. Medical Physics, 2017, 44, 6239-6250.	3.0	3
40	Data sustained misalignment correction in microscopic cone beam CT via optimization under the Grangeat Epipolar consistency condition. Medical Physics, 2020, 47, 498-508.	3.0	3
41	Three material decomposition for spectral imaging without contrast agents in photon-counting CT–Modeling and feasibility study. , 2020, , .		3
42	Impact of Overlying Personal Items on CT Dose with Use of Automated Tube Current Modulation—Pilot Investigation. Current Problems in Diagnostic Radiology, 2020, 49, 29-33.	1.4	1
43	Photonâ€counting CT via interleaved/gapped spectral channels: Feasibility and imaging performance. Medical Physics, 2021, , .	3.0	1
44	An efficient cone beam filtered back-projection (CB-FBP) reconstruction algorithm for a circle-plus-two-arc orbit. , 0, , .		0
45	The property of signal-to-noise and its variation over spatial frequency in differential phase contrast CT. , 2012, , .		0
46	Differential phase contrast CT — Characterics of signal and noise. , 2012, , .		0
47	Image-domain correction for gray level variation in circular cone-beam CT. , 2015, , .		0
48	Z-range Extension of Volume Imaged with Clinical C-arm Computed Tomography from A Single Rotation Helical Cone-beam Scan. , 2019, , .		0
49	Data acquisition with interleaved/gapped spectral channelization for spectral imaging in photon-counting CT. , 2022, , .		0